U. S. DEPARTMENT OF THE INTERIOR
U. S. GEOLOGICAL SURVEY

PROCESSING OF SEISMIC TOMOGRAPHY DATA COLLECTED AT TUNNEL 160, DEGELEN MOUNTAIN, KAZAKHSTAN

by

Karl J. Ellefsen[1] and William Leith[2]

Open-File Report 99-532

This report is preliminary and has not been reviewed for conformity to U. S. Geological Survey editorial standards. Any use of trade, product, or firm names is for descriptive purposes only and does not imply endorsement by the U. S. Government.

---

[1] U. S. Geological Survey, MS 964, Box 25046, Denver, CO 80225

[2] U. S. Geological Survey, 955 National Center, Reston, VA 20192

1999

ABSTRACT

At Degelen Mountain in Kazakhstan, seismic data were collected between the ground surface and tunnel 160, and the travel times of the *P*-waves were processed with tomographic methods to estimate the velocities. Most of the estimated velocities were between 4000 and 5150 m/s. The tomogram showed two distinct regions with low velocities: One region was near the tunnel between 216 and 270 m, horizontal distance (measured from the tunnel portal). The other region was near the ground surface between 310 and 424 m, horizontal distance; this particular region had the lowest velocities in the tomogram. An analysis of the resolution indicated that the smallest features that could be detected were about 18 m across. Near the middle of the tomogram, features were well resolved in the horizontal direction but just moderately resolved in the vertical direction. Near the edges of the tomogram, features were poorly resolved.

CONTENTS

LIST OF FIGURES

LIST OF TABLES

1. INTRODUCTION

During September 1999, a unique seismological experiment was conducted at the former Soviet nuclear test site at Degelen Mountain, which is in eastern Kazakhstan. For this experiment, code-named *Omega-2*, a 100-ton chemical explosion was used both to test technologies for monitoring the Comprehensive Nuclear Test Ban Treaty (CTBT) and to calibrate a portion of the CTBT's International Monitoring System. The *Omega-2* experiment, which was funded by the Department of Defense's Cooperative Threat Reduction Program, was conducted in conjunction with the closure of nuclear test tunnels and boreholes at the former Soviet nuclear test site (Leith and Kluchko, 1998). The *Omega* series experiments are specifically designed to evaluate technologies for monitoring nuclear tests; this calibration explosion is one of several, treaty-defined, confidence-building measures (Leith and others, in press).

The *Omega-2* experiment was fielded in tunnel 160, one of the many tunnels excavated into the flanks of Degelen Mountain. This tunnel, which is on the western side of the mountain, was excavated by the Soviets in the mid-1980's for an experiment to test the underground effects of two, 500-ton, chemical explosions. Because of its lack of radioactive contamination and its convenient location, this tunnel was selected by the Defense Threat Reduction Agency for the *Omega-2* experiment.

To gain some information about the effects of the explosion on the rock near tunnel 160, seismic data were collected both before and after the chemical explosion. (The collection was done by the Institute of Geophysical Research of the National Nuclear Center, which is in Kazakhstan.) A tomographic data set that was collected before the explosion probed the rock between the ground surface and tunnel 160. (This data set is known as profile 2, and the receivers in this profile extended from 216 to 378 m from the tunnel portal, as measured along the tunnel.) These data were transferred to the U. S. Geological Survey for processing, and in this report are the results of the processing.

2. FIELD DATA

The following information regarding the data collection is from "Seismic Tomography Report for Tunnel 160 (Report under contract DSWA01-98-C-0016-P0006 Item 0071)" and from informal, electronic mail. Sixteen shots, each consisting of 1 Kg explosives, were located at or near the ground surface. The seismic waves were detected by twenty-four ISN-01-24 seismic stations (that is, receivers) that were placed in holes in the left sidewall of tunnel 160. (The component of motion to which these receivers were sensitive is not known.) The locations of the shots and the receivers are listed in Tables 1 and 2 and are plotted in Figure 1. These locations include only elevation and horizontal distance — the sources and the receivers were practically in a vertical plane, and deviations from this plane were negligible.

The data were recorded by an SV-20-V seismograph, for which the sample rate was 0.5 ms and the number of samples was 681. Some seismograms had glitches (that is,

spikes) whose amplitudes were much higher than the amplitudes of the seismic waves; the glitches were removed with a 3-point median filter. The filtered seismograms from shot 1 are shown in Figure 2. In every seismogram, the first-arriving wave is interpreted as a *P*-wave that propagated directly from the source to the receiver.

Examine seismograms 1 through 16 from shot 1 (Figure 2). Some portions of these seismograms look like a square wave, indicating that the digitizer on the seismograph was saturated by a high-amplitude wave. The likely reason for the high amplitude wave was that the receivers were close to the shot. In seismograms 17 through 24, the amplitude of the initial *P*-wave was very small — it could not be discerned in the seismograms without automatic gain control. In seismogram 4, the character of the *P*-wave was unlike that in the seismograms on either side. This anomaly might have been caused by poor coupling between the receiver and the tunnel wall or by a malfunction in the electronics of the seismograph. In seismogram 16, the travel time of the *P*-wave was much less than the travel times for the seismograms on either side. This anomalous time might have been caused by a malfunction in the electronics of the seismograph. The problems in the seismograms from shot 1 were also observed in the seismograms from the other shots.

3. DATA PROCESSING

3.1 Picking Travel Times

Travel times of the *P*-waves were picked manually (that is, by eye) from a display on a computer screen; although this method was slow, its advantage was that unreliable travel times, which were usually caused by low amplitude *P*-waves, were readily detected and deleted.

To check the travel times, they were reduced — travel times for a homogeneous model (in which the rays were straight) were subtracted from the picked times. Then these reduced times were plotted (Figure 3). Usually, reduced times should change gradually between adjacent receiver numbers and similarly between adjacent shot numbers. An abrupt change indicated that a travel time pick might have been inaccurate. In such cases, the travel time was deleted, or a more accurate time was picked, or the original time was kept if it appeared reliable. Then another plot of the reduced travel times was made. After three iterations of this procedure, the reduced travel times appeared acceptable. The error in the picked times was estimated to be less than 1 ms, which corresponded to 2 sample points.

Of the 384 travel times, which came from the 384 seismograms, only 222 were deemed acceptable for further processing. These were often associated with high-amplitude *P*-waves.

3.2 Inversion

Velocities were estimated using geophysical inversion. The mathematical model for the inversion represented the rock as perfectly elastic, heterogeneous, isotropic, and

two-dimensional. Only a two-dimensional model was needed because the shots and the receivers were in a common plane. The coordinate system for this model was chosen to coincide with the coordinate system used for the shots and the receivers (Tables 1 and 2): The x axis corresponded to the horizontal direction, and the z axis to the vertical direction.

The inversion was implemented with a rectangular grid of points that were within the x-z plane (Figure 1). To each point in the grid, a velocity was assigned. In between the points, velocities were calculated via linear interpolation (Block, 1991, p. 21). The distance between the points was chosen to be 6 m. (Because the average velocity was roughly 4500 m/s and the maximum frequency in the P-waves was estimated to be 250 Hz, the minimum wavelength was roughly 18 m. Because the minimum wavelength approximately equals the size of the smallest heterogeneity that can be resolved with tomography (Williamson and Worthington, 1993), the distance between the points in the inversion grid should have been approximately 18 m. However, to account somewhat for the weathered bedrock near the ground surface, the grid spacing was reduced to 6 m.)

The inversion was based on a cost function that had two terms:

$$c = [\mathbf{d} - \mathbf{g}(\mathbf{m})]^T [\mathbf{d} - \mathbf{g}(\mathbf{m})] + \lambda [\mathbf{Km}]^T [\mathbf{Km}] , \qquad (1)$$

where T denotes transpose. In the first term, vector **d** contained the picked travel times; vector **g(m)** contained the predicted travel times that were calculated with ray tracing (Um and Thurber, 1987) for model **m**, the velocities at the grid points. The differences between the picked and the predicted travel times, the residuals, also formed a vector; because of the multiplication of this vector with itself, the first term was the sum of the squares of the residuals. In the second term, matrix **K** was an operator for calculating first derivatives in both the horizontal and the vertical directions. The product **Km** was a vector containing the first derivatives of the velocities in the model. (In addition, the derivatives in the x direction were multiplied by 3. This weighting, which constrained variations in the velocity, was necessary because of the small distances between the grid points.) Because of the multiplication of **Km** with itself, the second term was a measure of the roughness of the model. The scalar λ controlled the contribution of the roughness to the cost. Thus, the effect of minimizing c was to find, for the chosen λ, the velocities that made both the residuals and the roughness small.

Using the method of least squares (Lines and Treitel, 1984), c was minimized for many different values of λ. Two important quantities from each minimization were the square roots of the two terms in the cost function, called the rms (root mean square) residual and rms roughness. (The rms roughness did not include λ.) These two quantities were cross-plotted (Figure 4). For large values of λ (for example, 10), a small increase in the rms roughness was associated with a large decrease in the rms residual — essentially more information was extracted from the data. At the other extreme, for small values of λ (for example, 0.03), a large increase in the rms roughness was associated with in a small decrease in the rms residual — essentially the velocities were fit to noise in the data. Between these two extremes, where λ was 0.3, was the desired solution.

The velocities on the inversion grid were contoured (Figure 5a). Omitted from this contour map, or tomogram, were those regions lacking rays (for example, the upper left corner of the grid in Figure 1) because in such regions the velocities were unknown. Most of the estimated velocities are between 4000 and 5150 m/s. The tomogram shows two distinct regions with low velocities: One region is near the tunnel between 216 and 270 m, horizontal distance (measured from the tunnel portal). The other region is near the ground surface between 310 and 424 m, horizontal distance; this particular region has the lowest velocities in the tomogram. To check the minimization, the travel time residuals were plotted (Figure 5b). In general, the residuals are small compared to the sample rate (0.5 ms). However, the pattern formed by the residuals is non-random: The central part of the plotted residuals is blue, whereas the edges are red. This non-random pattern is characteristic of anisotropic rock (Chapman and Pratt, 1992; Pratt and Chapman, 1992; Pratt and others, 1993).

4. DISCUSSION

4.1 Resolution

To characterize the bedrock at Degelen Mountain, low velocities are especially important because they could be associated with either fracture zones or faults. To determine how well such regions could be detected with the tomographic data, a property called resolution, two numerical experiments were performed.

For these experiments, the low velocity regions were chosen to be squares for which the sides were 18 m long, because the smallest possible region that could be detected under ideal circumstances was approximately 18 m across (see Section 3.2). The velocities inside the squares were 4000 m/s and the squares were embedded in a medium with a velocity of 4500 m/s. For one experiment, the model had two low velocity regions (Figure 6a), and their locations were the same as those in the tomogram from the field data (Figure 5a). For the other experiment, the model had three low velocity regions that were located roughly halfway between the shots and the receivers (Figure 7a). For both models, the travel times were calculated with a finite difference method (Podvin and Lecomte, 1991). Using only those travel times for which there were a corresponding travel times in the field data, the velocities on the inversion grid (Figure 1) were estimated via the procedure described in Section 3.2. Only the tomograms for $\lambda = 0.3$ are presented because, for the field data, the tomogram for $\lambda = 0.3$ was selected as the desired solution. For both experiments, the travel time residuals were less than 0.5 ms, in magnitude, (which was the sample rate for the field data), and the residuals were practically random.

In both experiments, all low velocity regions were detected (Figures 6b and 7b). However, the estimated velocities within these regions were higher than the corresponding velocities in the starting model. The reason for these high estimates was that the velocities were constrained by the second term of the cost function (Equation 1).

The low velocity zone near the middle (300 m horizontal distance and 690 m elevation in Figure 7b) was elongated in the vertical direction. The other low velocity zones, which were all near the edges (less than 240 m and greater than 360 m horizontal distance), were very distorted.

To understand the reason for the distortion, examine the ray coverage (Figure 8). (The ray coverage for both numerical experiments was identical to that for the field data.) Near the middle, many rays were vertical or almost vertical, and consequently the velocity anomaly near the middle (Figure 7b) was well resolved in the horizontal direction. Because these rays had only a small component in the horizontal direction, the velocity anomaly was just moderately resolved in the vertical direction. Near the edges, there were only a few rays, and they were mostly vertical. Therefore, the velocity anomalies here were poorly resolved.

These two numerical experiments have several implications for delineating fracture zones or faults with the tomographic data. First, fracture zones or faults that were roughly 18 m across would be detected with these data. Second, the estimated velocities would not be as low as those in the rock because the inversion algorithm constrained the velocity changes. Third, if the fracture zone or fault were near the middle (between 240 and 360 m, horizontal distance), the shape shown in the tomogram would be somewhat elongated in the vertical direction. If the fracture zone or fault were near the edges (less than 240 m or greater than 360 m, horizontal distance), the shape would be very distorted

4.2 Other Issues

The pattern shown in the travel time residuals (Figure 5b) indicates that the rock may be anisotropic in its elastic properties. Such anisotropy in igneous and metamorphic rocks may be caused by fracturing or alignment of the constituent minerals (Nur and Simmons, 1969; Thill and others, 1973; Lo and others, 1986). Hence, characterizing the seismic anisotropy with the ultimate goal of determining fracture properties would appear to be a desirable goal. To accomplish this, seismic waves must propagate through rock in all possible directions within a three-dimensional volume. However, for this investigation, the shots and the receivers were restricted to a two-dimensional plane (Figure 1); moreover, within this plane, the rays were either vertical or inclined — none were horizontal (Figure 8). Consequently, the rock was not probed in enough directions to characterize the anisotropy.

The geophysicists from The National Nuclear Center worked diligently, under difficult conditions, to collect the seismic data. In an effort to help them collect even better data in the future, the following ideas are offered for their consideration. (1) Portions of some seismograms looked like a square wave probably because the digitizer on the seismograph was saturated. This problem would be either diminished or eliminated if a seismograph with a greater dynamic range were used. (2) The travel times from some seismograms were too small compared to the travel times from adjacent seismograms. These anomalous times might have been caused by an electronics problem in the seismograph, and so the

seismograph should be checked. (3) The character of the *P*–wave in some seismograms differed markedly from the character in adjacent seismograms. Although there could be several different causes for this change in character, a common cause would be poor mechanical coupling between the receiver and the rock. The coupling should be checked carefully.

4.3. Future Work

As part of the *Omega-2* experiment, additional seismic data have been collected, and these data could substantially improve the characterization of the rock above the tunnel complex. Here are four specific suggestions:

- The data from the second profile (which is presented in this report) should be processed simultaneously with the data from the first profile. [These other data were described in "Seismic Tomography Report for Tunnel 160 (Report under contract DSWA01-98-C-0016-P0006 Item 0071)."]. The first and the second profiles overlap somewhat, and consequently the resolution of the velocities using the combined profiles would be better than the resolution using separate profiles.

- The low velocities near the ground surface should be determined independently of the tomographic inversion and then used as constraints in the inversion. This procedure would improve the estimates of the velocities above the tunnel. Indeed, the low velocities probably can be estimated from some seismic refraction data, which were recently collected on the ground surface, just above the tunnel complex.

- The seismic data collected between tunnel 160 and tunnel 160-B should be processed. (Tunnel 160-B, which was excavated in 1999, is 20 meters above tunnel 160). This particular profile has a dense array of shots and receivers, and the estimated velocities could provide valuable information about this important region between the two tunnels.

- Information about attenuation should be extracted from the seismic data because such information will help characterize the fracturing due to the explosion. (That is, fractures attenuate seismic waves. By estimating the spatial variations in the attenuation, the spatial variations in the rock fracturing can be inferred.) Extracting information about attenuation would be very difficult because some seismograms were saturated, the coupling between the receivers and the rock probably varied along the profile, and similarly the coupling between each shot and the rock probably varied along the profile.

5. ACKNOWLEDGEMENTS

The National Nuclear Center at the Kazakhstan Institute of Geophysical Research provided the seismic data to the U. S. Geological Survey. Dr. Valery Demin and Alexander Smirnov were

especially helpful in answering many questions about the data. This work was supported by the Defense Threat Reduction Agency, under IACRO 99-3014.

6. REFERENCES

Block, L. V., 1991, Joint hypocenter-velocity inversion of local earthquake arrival time data in two geothermal fields, PhD thesis, Massachusetts Institute of Technology, 448 p.

Chapman, C. H. and Pratt, R. G., 1992, Traveltime tomography in anisotropic media—I. Theory: Geophysical Journal International, v. 109, p. 1–19.

Lines, L. R., and Treitel, S., 1984, A review of least-squares inversion and its application to geophysical problems: Geophysical Prospecting, v. 32, p. 159–186.

Leith, W., and Kluchko, L. J., 1998, Seismic experiments, nuclear dismantlement go hand-in-hand in Kazakhstan, EOS Trans. AGU, v. 79, n. 37, p. 443-444.

Leith, W., Kluchko, L. J., and Konovalev, V., Ongoing Research Experiments at the Former Soviet Nuclear Test Site in Eastern Kazakhstan, in Proc. 9th Int. Conf. Rock Mechanics, Elsevier, Amsterdam, *in press*.

Lo, T., Coyner, K. B., and Toksöz, M. N., 1986, Experimental determination of elastic anisotropy of Berea sandstone, Chicopee shale, and Chelmsford granite: Geophysics, v. 51, p. 164–171.

Nur, A., Simmons, G., 1969, Stress-induced velocity anisotropy in rock: An experimental study: Journal of Geophysical Research, v. 74, p. 667-6674.

Podvin, P., and Lecomte, I., 1991, Finite difference computation of traveltimes in very contrasted velocity models: a massively parallel approach and its associated tools: Geophysical Journal International, v. 105, p. 271–284.

Pratt, R. G., and Chapman, C. H., 1992, Traveltime tomography in anisotropic media—I. Application: Geophysical Journal International, v. 109, p. 20–37.

Pratt, R. G., McGaughey, W. J., and Chapman, C. H., 1993, Anisotropic velocity tomography: A case study in a near-surface rock mass: Geophysics, v. 58, p. 1748–1763.

Thill, R.E., Bur, T. R., and Steckley, R. C., 1973, Velocity anisotropy in dry and saturated rock spheres and its relation to rock fabric: Int. J. Rock Mech. Min. Sci. & Geomech. Abstr., v. 10, p. 535–557.

Um, J., and Thurber, C., 1987, A fast algorithm for two-point seismic ray tracing: Bulletin of the Seismological Society of America, v. 77, p. 972–986.

Williamson, P. R., and Worthington, M. H., 1993, Resolution limits in ray tomography due to wave behavior: Numerical experiments: Geophysics, v. 58, p. 727–735.

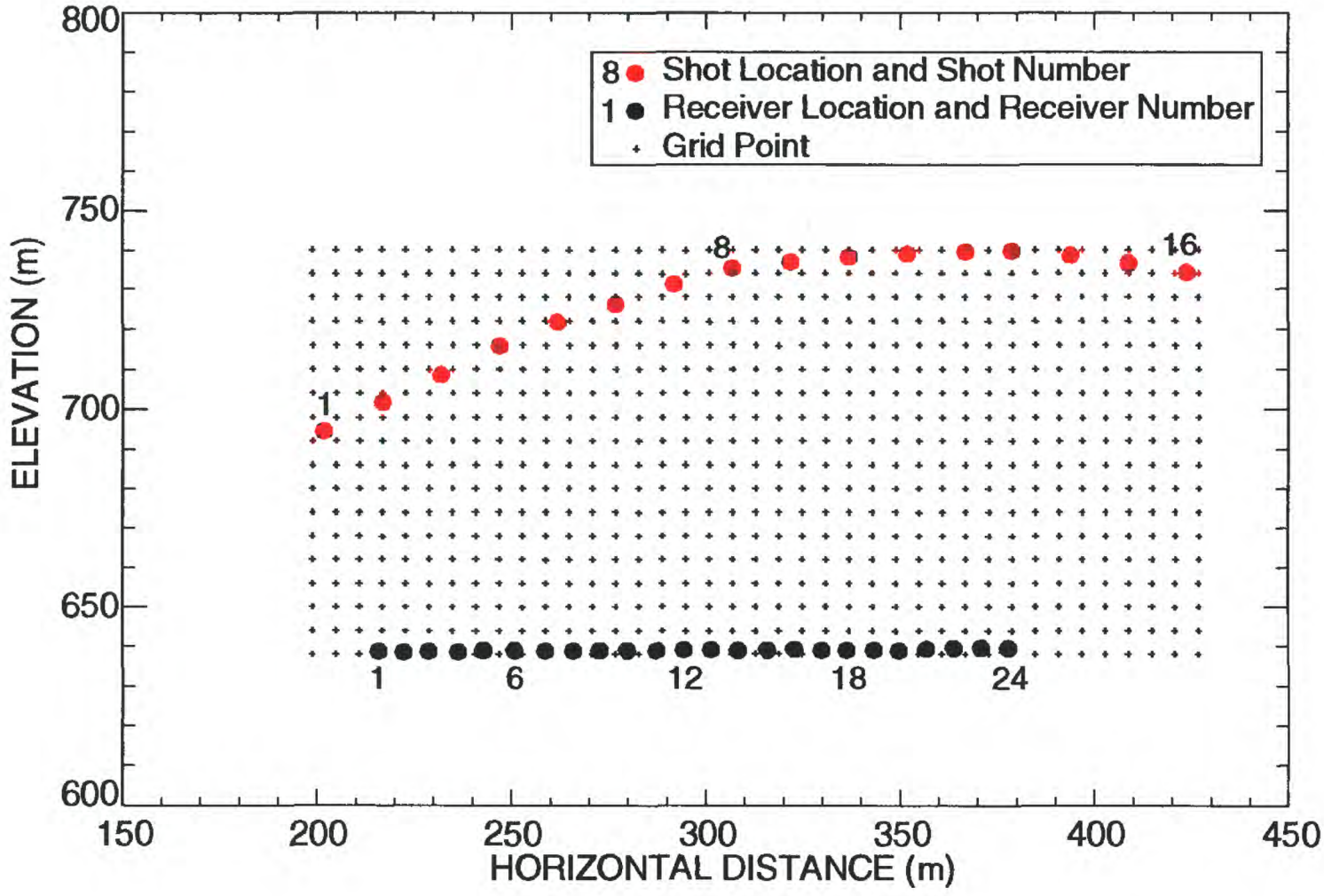

Figure 1. Shot locations, receiver locations, and the grid used for the inversion.

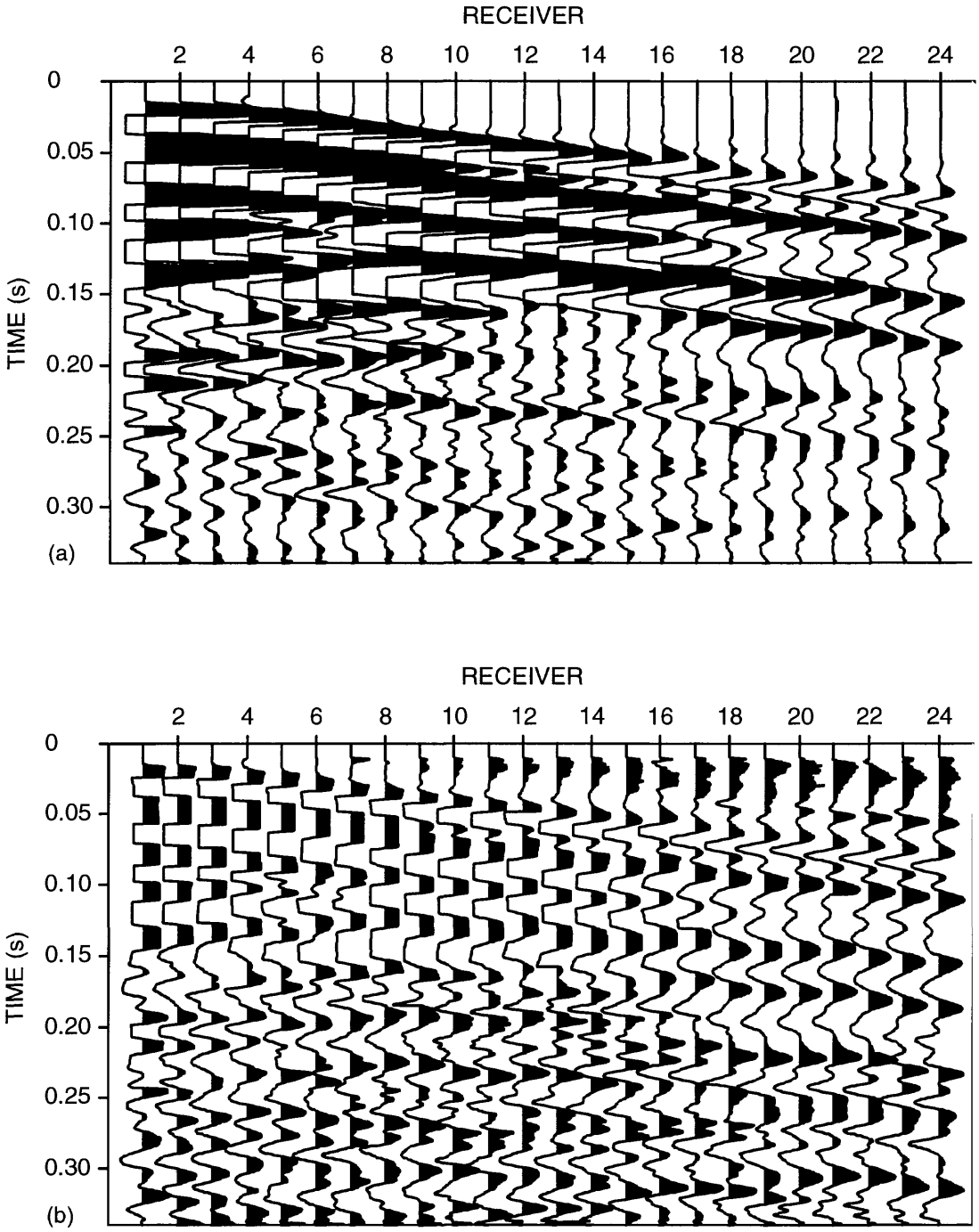

Figure 2. Seismograms from shot 1 (a) after median filtering and (b) after median filtering and amplitude scaling (using automatic gain control with a 0.03 s window).

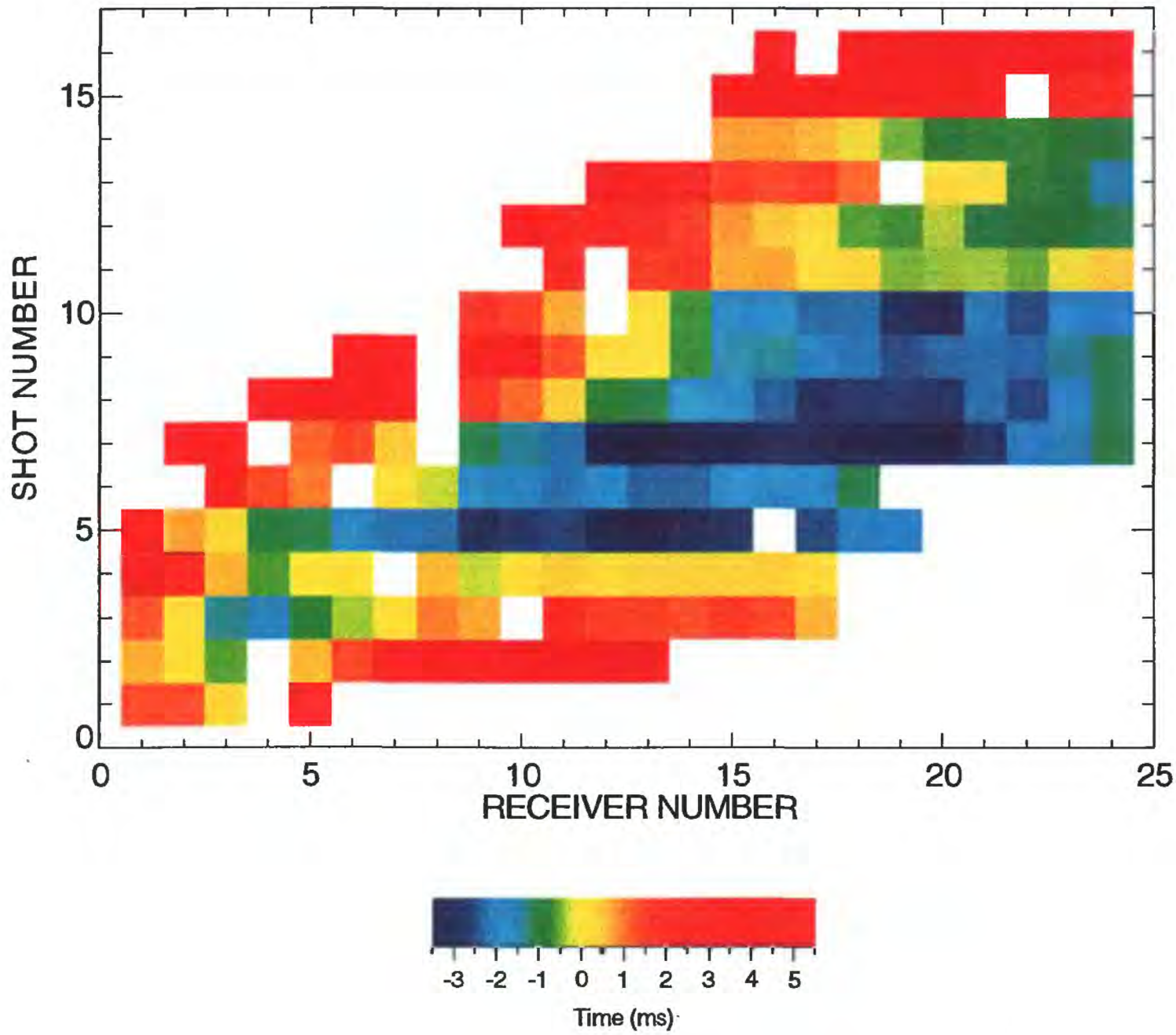

Figure 3. Reduced travel times after three checks of the picked travel times.

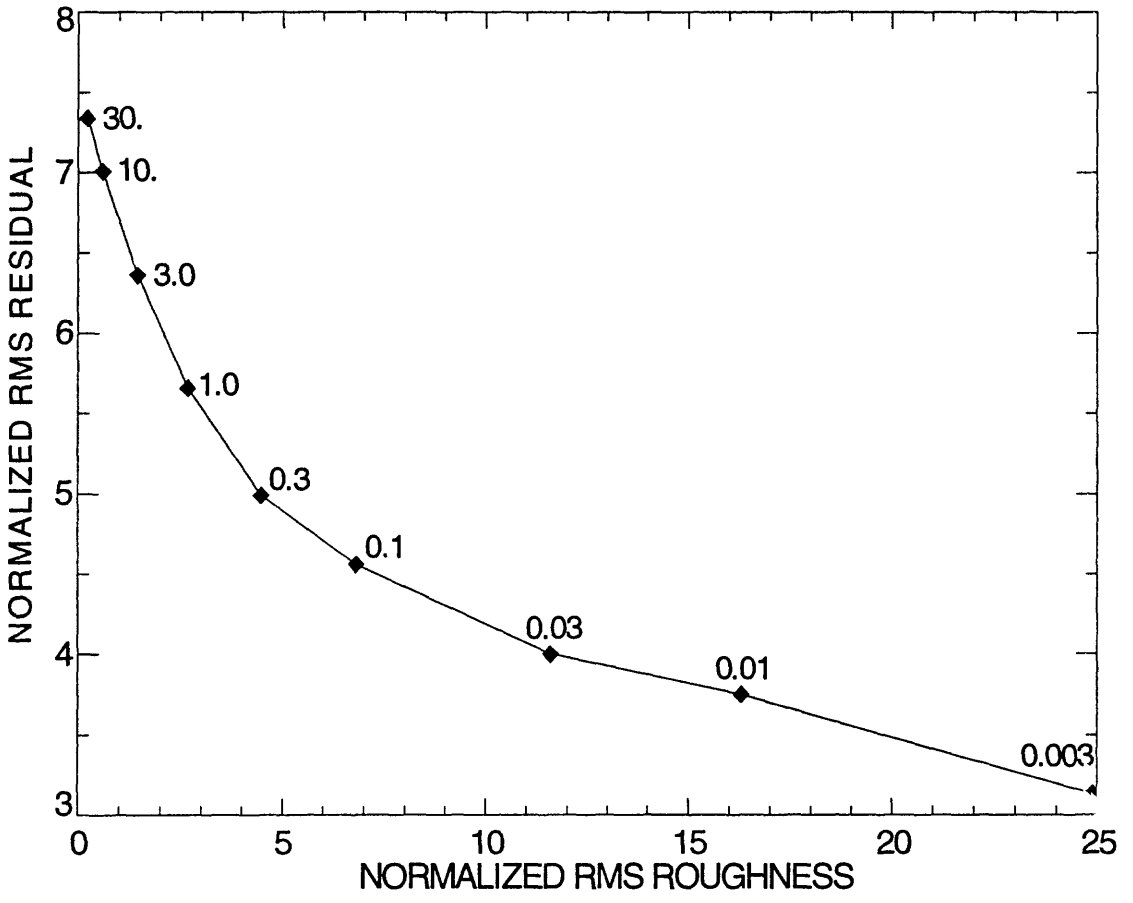

Figure 4. Normalized rms residual and the normalized rms roughness from each inversion. The number adjacent to each data point is λ.

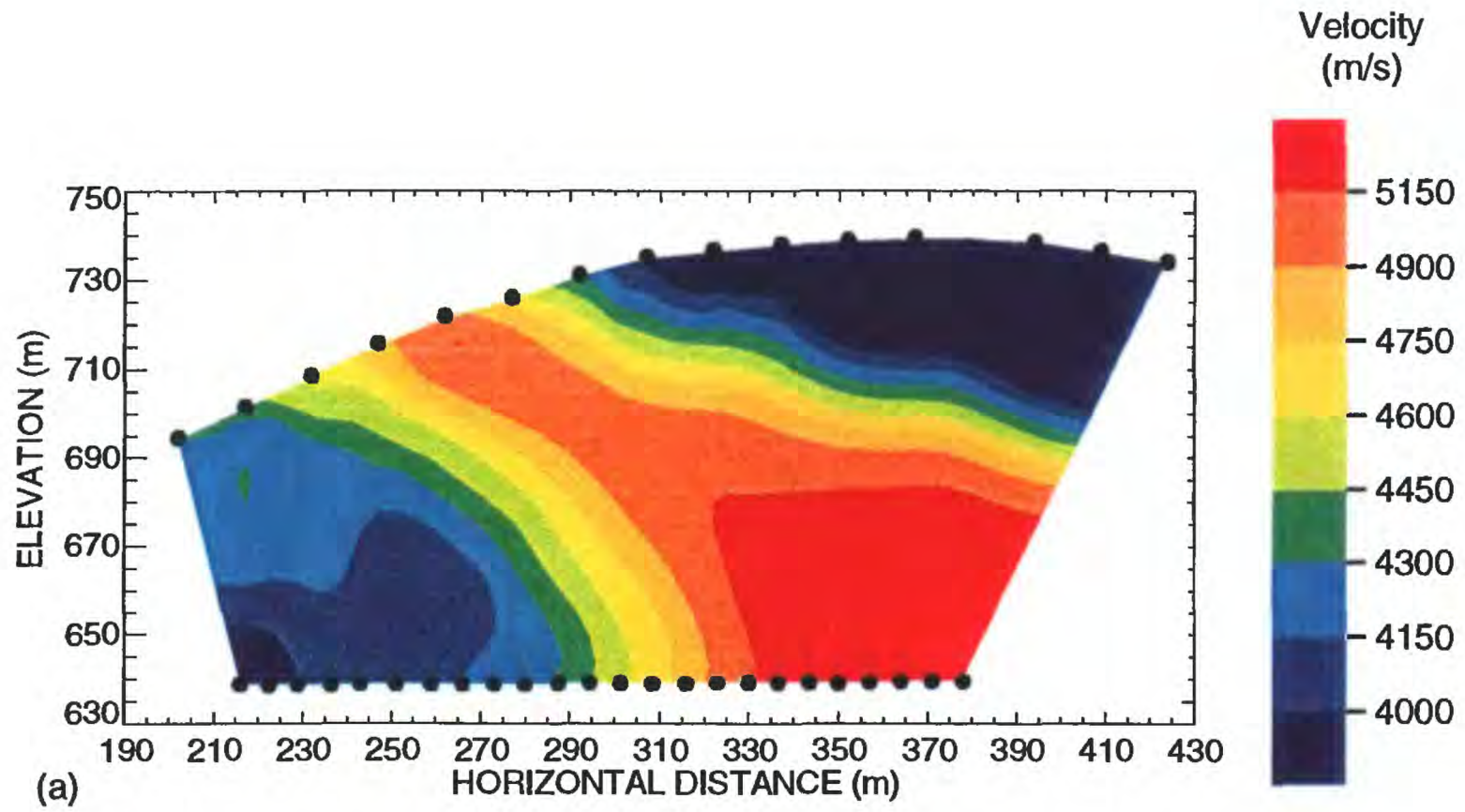

Figure 5. (a) Tomogram and (b) travel time residuals for the inversion with $\lambda = 0.3$.

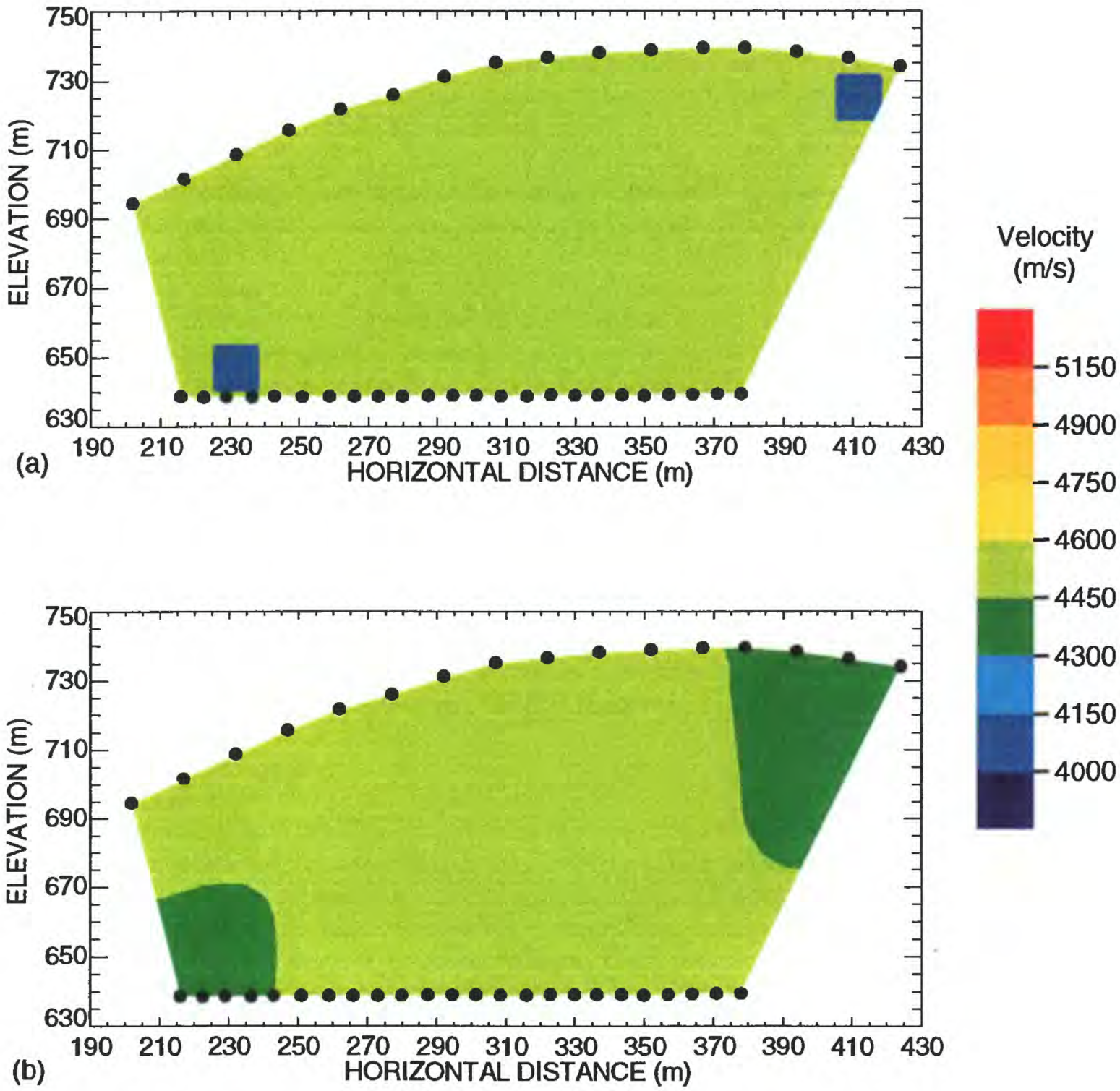

Figure 6. (a) Starting model and (b) tomogram used to determine the resolution of the tomographic data. The two low velocity regions were in the same locations as those in the tomogram from the field data (Figure 5a). See also Figures 7 and 8.

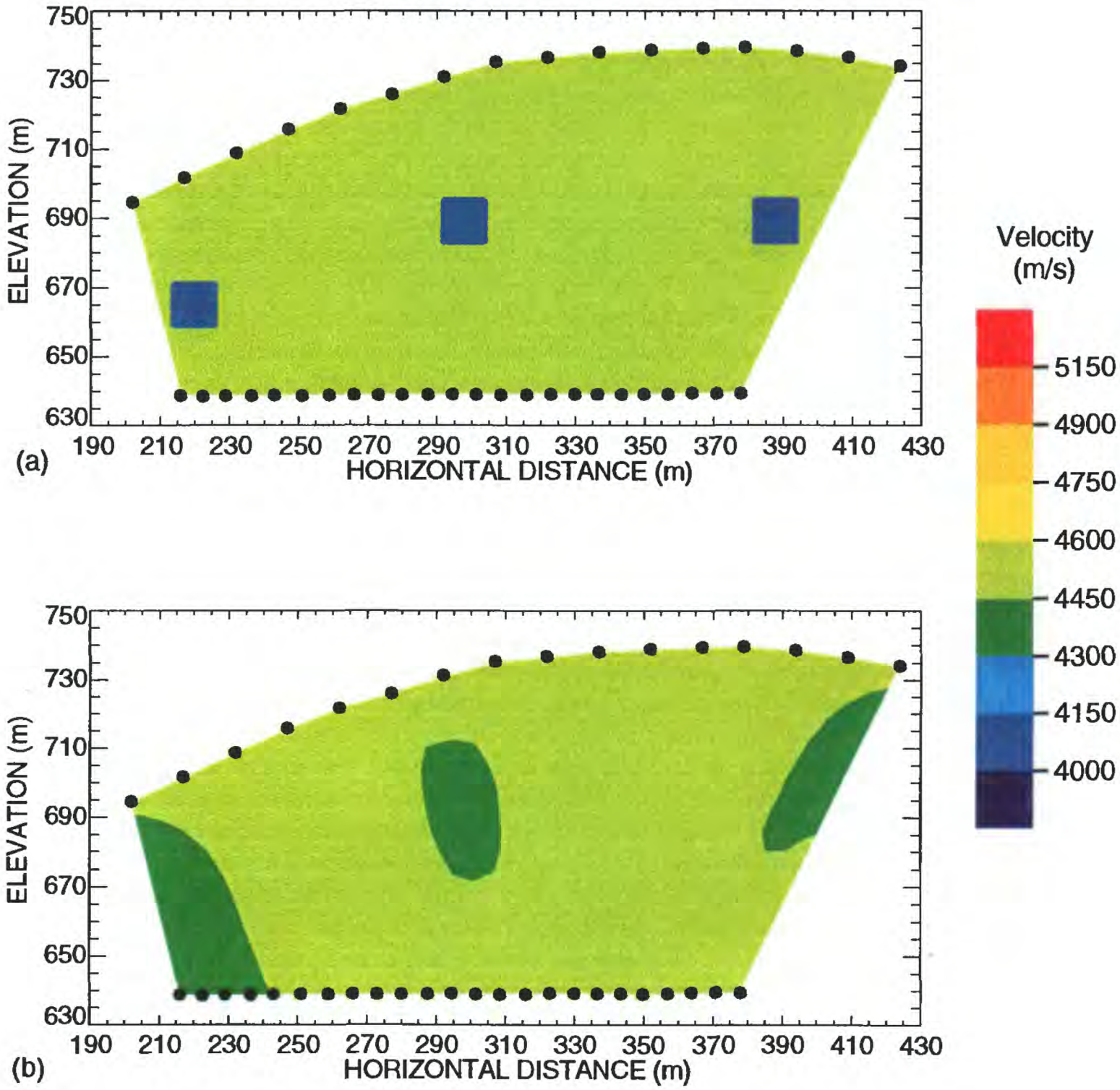

Figure 7. (a) Starting model and (b) tomogram used to determine the resolution of the tomographic data. See also Figures 6 and 8.

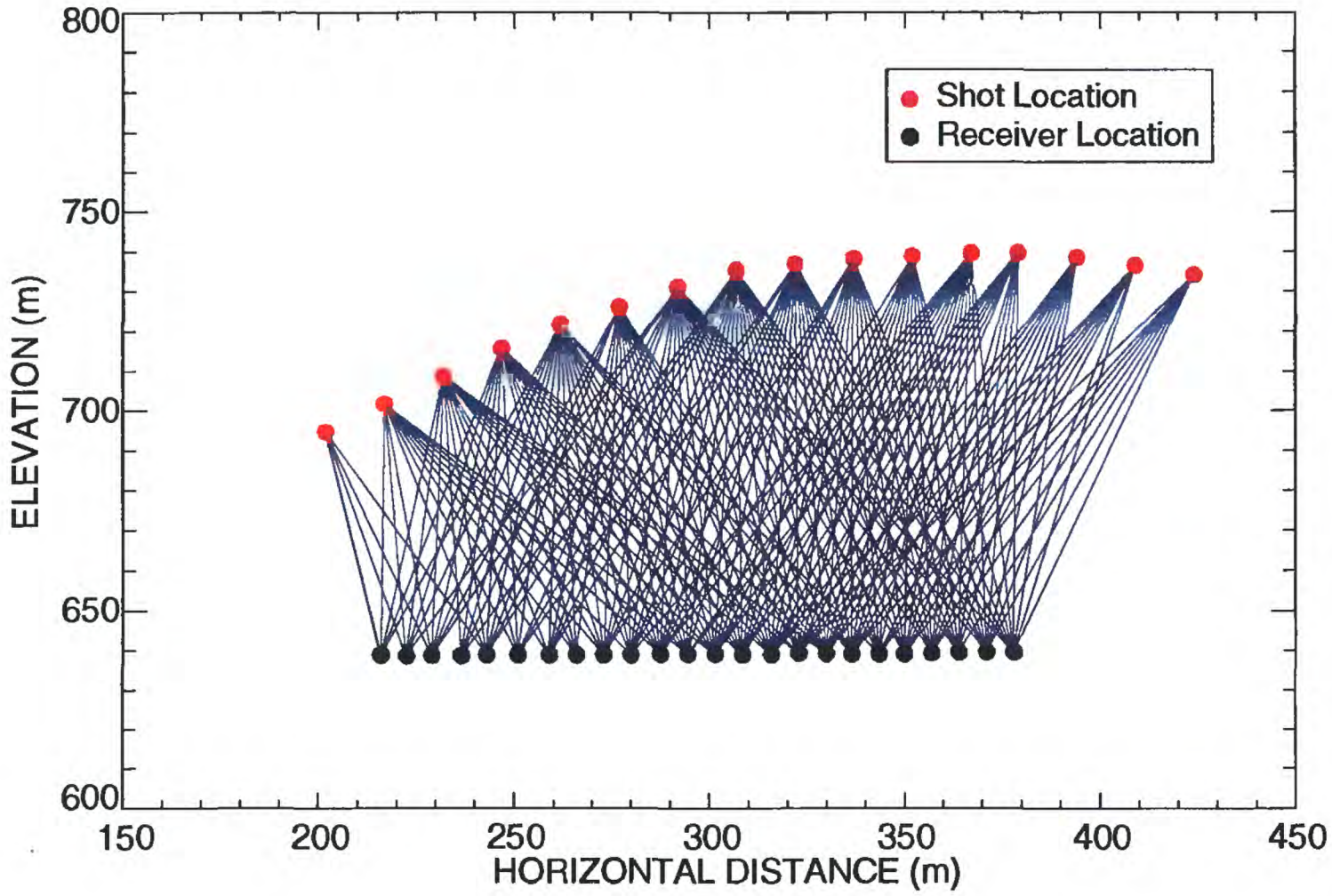

Figure 8. Ray coverage for the field data and for the two numerical experiments used to determine the resolution. Each ray corresponds to one travel time that was used in the inversions for the velocities (Figures 5a, 6b, and 7b).

Table 1. Locations of the shots. Horizontal distance was measured from the portal of tunnel 160. The file names refer to the digital files in which the data are stored (as common shot gathers). The precision of the elevations differs from that of the horizontal distances; the reason is not known.

Shot Number	Elevation (m)	Horizontal Distance (m)	File name
1	694.5	202.	k1b5
2	701.58	217.	k1b4
3	708.63	232.	k1b3
4	715.69	247.	k1b2
5	721.69	262.	k1b1
6	726.05	277.	k1a13
7	731.06	292.	k1a12
8	735.24	307.	k1a11
9	736.74	322.	k1a10
10	738.06	337.	k1a9
11	738.77	352.	k1a8
12	739.41	367.	k1a7
13	739.55	379.	k1a6
14	738.45	394.	k1a5
15	736.43	409.	k1a4
16	734.09	424.	k1a3

Table 2. Locations of the receivers. Horizontal distance was measured from the portal of tunnel 160. The precision of the elevations differs from that of the horizontal distances; the reason is not known.

Receiver Number	Elevation (m)	Horizontal Distance (m)
1	638.74	216.
2	638.48	222.5
3	638.66	229.
4	638.6	236.5
5	638.	243.
6	638.78	251.
7	638.76	259.
8	638.81	266.
9	638.85	273.
10	638.83	280.
11	638.96	287.5
12	639.07	294.5
13	639.04	301.5
14	638.87	308.5
15	638.91	316.
16	639.2	323.
17	639.08	330.
18	639.06	336.5
19	639.07	343.
20	639.03	350.
21	639.22	357.
22	639.42	364.
23	639.52	371.
24	639.44	378.